

The Multiplicity Dependence of Pion Interferometry in Hydrodynamics

Christopher Plumberg^{1,*}

¹*Illinois Center for Advanced Studies of the Universe, Department of Physics,
University of Illinois at Urbana-Champaign, Urbana, IL 61801, USA*

(Dated: March 17, 2024)

Understanding the origins of collective, fluid-like behavior in ultrarelativistic nuclear collisions constitutes one of the biggest open challenges in the field. In this Letter, it is argued that certain features in the multiplicity dependence of the source sizes extracted using pion interferometry may be understood quite naturally if small systems evolve hydrodynamically at sufficiently large multiplicities. Interferometry may therefore provide a baseline for probing and constraining the nature of collective behavior in nuclear collisions.

1. Introduction. It is by now widely recognized that ultrarelativistic nuclear collisions exhibit collective, fluid-like behavior (or ‘collectivity’) [1, 2]. The current challenge is to understand what produces this behavior. To date, many different explanations of collectivity have been proposed [3–12]. In order to experimentally discriminate between these proposals, one needs a set of observables which can probe the consequences of collective behavior in highly specific and non-trivial ways.

Collectivity is commonly defined by strong space-momentum correlations [13]. As such, it should manifest itself in both momentum-space and coordinate-space observables [14]. An ideal way to probe the latter in nuclear collisions is provided by Hanbury Brown–Twiss (HBT) interferometry and the observables derived from it, the ‘HBT radii’ [15, 16].

The HBT radii reflect collectivity in a number of ways, including their dependence on the transverse pair momentum K_T and the system’s charged multiplicity $dN_{\text{ch}}/d\eta$. However, although a fairly clean and extensive theoretical structure exists for understanding the former [17, 18], somewhat less attention has been paid to quantitatively extracting insights from the latter, although important work has been done on this as well [16, 19].

For a thermalized, hydrodynamic medium, one expects the spatial volume of the system to scale approximately linearly with the multiplicity $dN_{\text{ch}}/d\eta$, suggesting that the individual radii scale linearly with $(dN_{\text{ch}}/d\eta)^{1/3}$ [16]. This rough expectation has been abundantly confirmed in experimental data [20–22]. However, there are two significant features of the $(dN_{\text{ch}}/d\eta)^{1/3}$ -dependence in the radii which initially appear to contradict what one expects on the basis of hydrodynamic models. First, one observes that the slope of the $(dN_{\text{ch}}/d\eta)^{1/3}$ -scaling in each radius varies between large and small collision systems. I refer to this variation as a *slope non-universality* in the scaling of the radii across different size systems. Second, one finds that different radii exhibit different slopes in the *same* collision system. In the widely used out-side-long (o, s, l) coordinate system [23], for instance, with primary radii R_o , R_s , and R_l , the R_o slope tends to be considerably smaller than the R_s , R_l slopes in small

systems, whereas all three are roughly comparable in magnitude in larger systems [24–26]. There is thus a *slope hierarchy* between the respective radii whose magnitude depends on the collision system in which it is measured. Taken together, these two features – the hierarchy and non-universality in the slopes of the radii with $(dN_{\text{ch}}/d\eta)^{1/3}$ – appear initially to stand in tension with the hydrodynamic expectation that all radii should scale in similar ways across collision systems.

The goal of this Letter is to show that these experimental trends are in fact automatic consequences of hydrodynamic behavior and arise naturally in systems which exhibit anomalously strong collective flow. A simple model is used to explore heuristically the qualitative behavior of the different HBT radii in hydrodynamics as a function of system size and multiplicity and to show what this implies about the underlying space-time evolution of the systems in question. A systematic and quantitative analysis of the HBT radii and their multiplicity dependence may therefore elucidate the nature of collectivity in crucial ways and open up novel avenues for exploring the mechanisms which drive the dynamical evolution of ultrarelativistic nuclear collisions.

2. Methodology. The starting point for HBT analyses is the two-particle correlation function:

$$C(\vec{p}_1, \vec{p}_2) = \frac{E_1 E_2 \frac{dN}{d^3 p_1 d^3 p_2}}{\left(E_1 \frac{dN}{d^3 p_1}\right) \left(E_2 \frac{dN}{d^3 p_2}\right)}. \quad (1)$$

It is constructed ideally to reduce to unity in the absence of Bose-Einstein or Fermi-Dirac correlations. In this Letter, this correlation function is computed and studied for pions produced by three different systems as functions of $(dN_{\text{ch}}/d\eta)^{1/3}$: p+p collisions at 7 TeV, p+Pb collisions at 5.02 TeV, and Pb+Pb collisions at 2.76 TeV.

In terms of the relative momentum q and the pair momentum K , defined by

$$q = p_1 - p_2, \quad K = \frac{1}{2} (p_1 + p_2), \quad (2)$$

one may parameterize the correlation function (1) in a

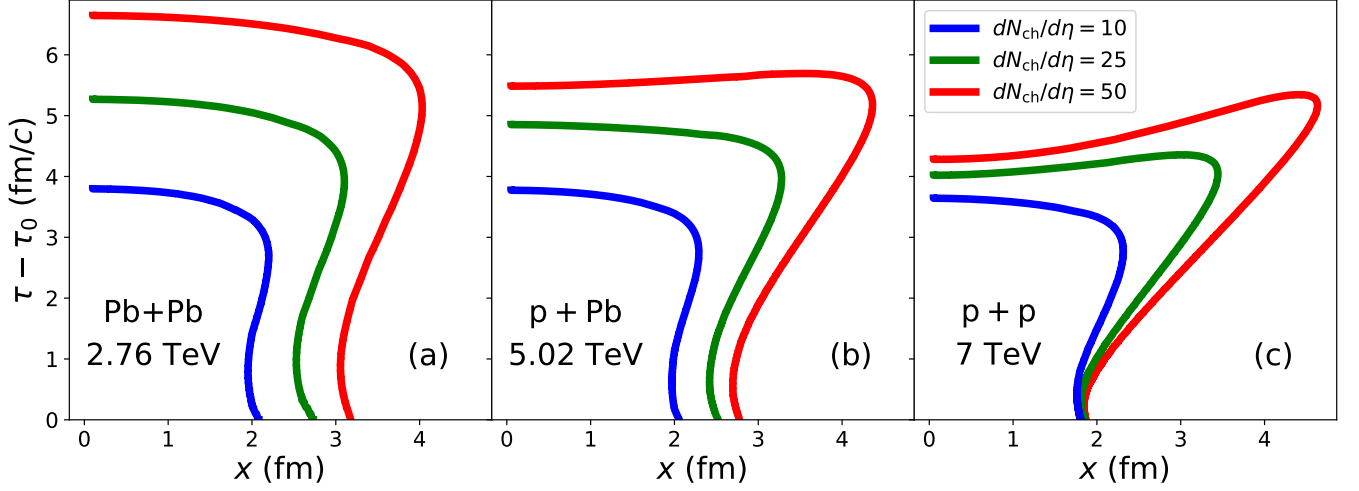


FIG. 1. Comparison of freeze-out surface slices (at $y = 0$) in Pb+Pb (a), p+Pb (b), and p+p (c) collision systems, for different fixed multiplicities of $dN_{\text{ch}}/d\eta = 10$ (blue, innermost contours), 25 (green, middle contours), and 50 (red, outermost contours). As noted in [27], the comoving volume of the freeze-out surface is fixed by the multiplicity, but the space-time volume enclosed by the freeze-out surface reflects the highly system-dependent spatial geometry and strength of collective flow.

form which is Gaussian in \vec{q} :

$$C_{fit}(\vec{q}, \vec{K}) = 1 + \lambda(\vec{K}) \exp \left(- \sum_{i,j \in \{o,s,l\}} R_{ij}^2(\vec{K}) q_i q_j \right), \quad (3)$$

where (o, s, l) label the respective axes of the out-side-long coordinate system [23], and I have specified to the case of pion (i.e., Bose-Einstein) correlations. The strength of the Bose-Einstein enhancement is absorbed into the normalization factor $\lambda(\vec{K})$, which may deviate from unity in the presence of resonance decays [28] and coherent pion production [29]. Here, I assume purely chaotic and thermal pion emission for simplicity, so that $\lambda(\vec{K}) = 1$. The inverse square widths of the enhancement are parametrized by the HBT radii $R_{ij}^2(\vec{K})$, which quantify the effective sizes (or ‘homogeneity lengths’ [17]) of regions in the system which dominate pair production at a given \vec{K} , and thereby convey a mixture of spatial and temporal information regarding the evolution and particle emission process of nuclear collisions.

In the case of a system whose pions are emitted according to a phase-space distribution S (or ‘source function’ [30]) which is Gaussian in its space-time dependence,¹ one can show that the following ‘pocket relations’ hold exactly [32]:

$$R_s^2 = \langle \tilde{x}_s^2 \rangle \quad (4)$$

$$R_o^2 = \langle \tilde{x}_o^2 \rangle - 2\beta_T \langle \tilde{x}_o \tilde{t} \rangle + \beta_T^2 \langle \tilde{t}^2 \rangle \quad (5)$$

$$R_l^2 = \langle \tilde{x}_l^2 \rangle - 2\beta_L \langle \tilde{x}_l \tilde{t} \rangle + \beta_L^2 \langle \tilde{t}^2 \rangle, \quad (6)$$

¹ This is a reasonable assumption for the thermal pion source used here [31].

where all averages are taken with respect to S and the shifted coordinates \tilde{x}^μ and pair velocity $\vec{\beta}$ are given by [18]

$$\tilde{x}^\mu = x^\mu - \langle x^\mu \rangle, \quad \vec{\beta} = \frac{\vec{K}}{K^0} \approx \frac{\vec{K}}{\sqrt{m_\pi^2 + \vec{K}^2}}. \quad (7)$$

Each of the terms in (4)-(6) characterizes a particular spatiotemporal dimension of the particle source S and is thus termed a ‘source variance’ [33]. Although the radii reported here are extracted by fitting (3) to the correlation function (1) as computed within a hydrodynamic approach, the relations (4)-(6) establish a connection between the R_{ij}^2 and the source variances which quantify the space-time structure of S , thereby reflecting the ‘freeze-out hypersurface’ at which hydrodynamics is terminated and the system is converted to particles [32].

For this work, the boost-invariant hydrodynamic framework iEBE-VISHNU [10] was used to model p+p collisions at 7 TeV, p+Pb collisions at 5.02 TeV, and Pb+Pb collisions at 2.76 TeV, using smooth, event-averaged MC-Glauber initial conditions [34]. The correlation function (1) was evaluated numerically in terms of integrals over each system’s freeze-out hypersurface with respect to the corresponding source function S . It was then fit as a function of \vec{q} and \vec{K} to the parameterization (3), thereby yielding the radii $R_{ij}^2(\vec{K})$. Further details of the hydrodynamic implementation used and the subsequent extraction of the radii have been given in Ref. [26].

3. Results. I now consider, using the hydrodynamic model just described, how the effects of collective flow may be manifested in the multiplicity dependence of pion interferometry. I first show the freeze-out hypersurfaces

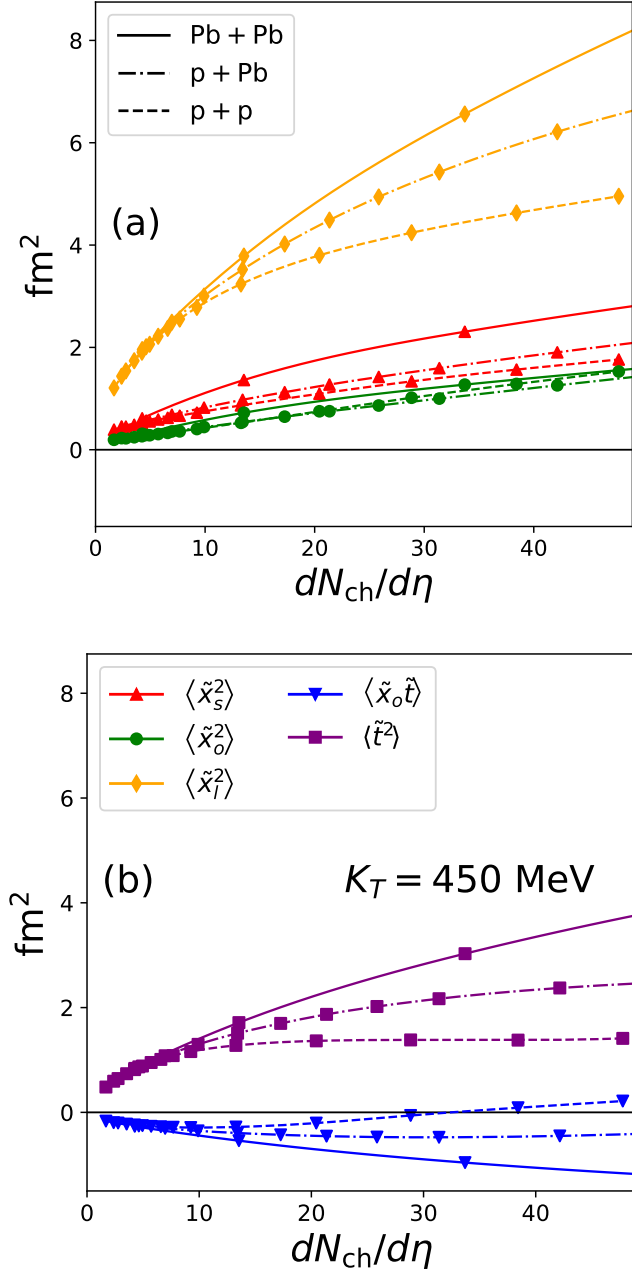


FIG. 2. The evolution of the space-time geometry, as reflected in the various terms entering the pocket relations (4)-(6) with $dN_{\text{ch}}/d\eta$. The geometric terms ($\langle \tilde{x}_s^2 \rangle$, $\langle \tilde{x}_o^2 \rangle$, $\langle \tilde{x}_l^2 \rangle$) scale monotonically with $dN_{\text{ch}}/d\eta$ in both large and small systems, whereas the terms sensitive to the temporal structure ($\langle \tilde{t}^2 \rangle$, $\langle \tilde{x}_o \tilde{t} \rangle$) exhibit radical differences in $dN_{\text{ch}}/d\eta$ -scaling between different collision systems.

themselves, followed by the source variances, and finally the radii as functions of $(dN_{\text{ch}}/d\eta)^{1/3}$.

3a. Freeze-out hypersurfaces. In Fig. 1, I show the freeze-out hypersurfaces obtained from each simulated collision system for different fixed multiplicities $dN_{\text{ch}}/d\eta = 10, 25, 50$. One finds that large systems and

small systems differ dramatically in their multiplicity dependence: whereas the former change mainly by a global rescaling of the enclosed space-time volume, with only minor changes to the overall shape, the latter simultaneously grow larger and become distorted in their shape with increasing $dN_{\text{ch}}/d\eta$ [19]. The distortions arising in small systems are driven primarily by enhanced collective flow, a consequence of the fact that small systems are created with substantially larger initial density gradients than large systems [26, 27].

In the highest multiplicity p+p and p+Pb collisions, one further notices a *reversal* of the order in which freeze out occurs in Pb+Pb: the center tends to freeze out *first* in small systems [cf. Fig. 1(b)-(c)], followed by the edges, whereas in large systems the center freezes out *after* the edges [cf. Fig. 1(a)]. This reversal in turn generates a strong, *positive* correlation in small systems between a given pion's x_o emission coordinate and the proper time τ at which the pion was produced. These features are again consequences of strong transverse expansion and lead to corresponding effects on the source geometry as probed by pion interferometry.

3b. Source variances. The evolution with $dN_{\text{ch}}/d\eta$ of the freeze-out hypersurfaces determines the corresponding behavior of the source function S and its space-time structure. This structure can be probed quantitatively by considering the various terms entering the pocket relations (4)-(6). In Fig. 2, we show the five terms which contribute to the radii in the LCMS frame, where $\beta_L \equiv 0$ [35, 36].

Fig. 2(a) reveals a monotonic growth in the geometric terms ($\langle \tilde{x}_s^2 \rangle$, $\langle \tilde{x}_o^2 \rangle$, $\langle \tilde{x}_l^2 \rangle$) with $dN_{\text{ch}}/d\eta$. This growth reflects the corresponding growth with multiplicity in the spatial sizes of the systems shown in Fig. 1; each freeze-out hypersurface must have the same co-moving volume at a fixed multiplicity, irrespective of the collision's enclosed space-time volume [27]. Fig. 2(b), by contrast, shows non-monotonic behavior in the temporal structure ($\langle \tilde{t}^2 \rangle$, $\langle \tilde{x}_o \tilde{t} \rangle$) of the source function S . This, too, is a direct consequence of the multiplicity scaling seen in Fig. 1. One observes that in small systems at large multiplicities, the emission duration $\langle \tilde{t}^2 \rangle$ flattens dramatically while the correlation term $\langle \tilde{x}_o \tilde{t} \rangle$ changes sign from negative to positive; both effects result from the elongated ‘wing-like’ structures visible in Fig. 1(b) and (c). By combining the scaling of the source variances together with the pocket relations (4)-(6), one is thus led to expect on the basis of hydrodynamics that the R_o scaling with $(dN_{\text{ch}}/d\eta)^{1/3}$ in small systems will be much weaker than that of R_s or R_l , whereas in large systems one expects to see a more uniform scaling in all radii [26].

3c. HBT radii. The multiplicity scaling of the source function S and its space-time structure ultimately determine the HBT radii extracted the correlation function (1). This is shown in Fig. 3 for the three radii and col-

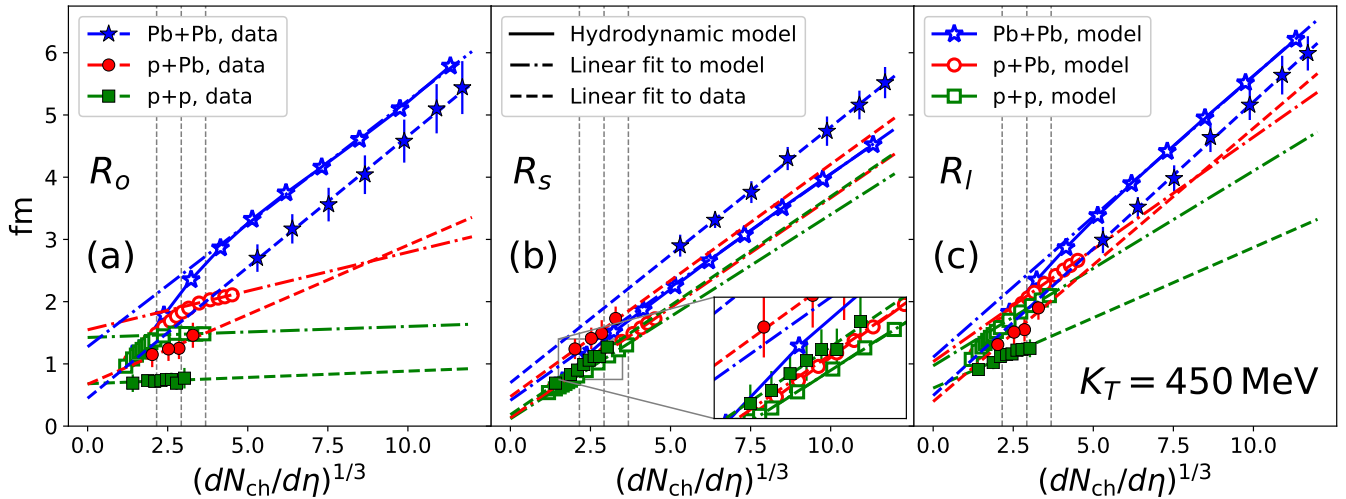


FIG. 3. Hydrodynamic calculations of the $(dN_{ch}/d\eta)^{1/3}$ -dependence in R_o (a), R_s (b), and R_l (c), compared with corresponding experimental measurements in p+p at 7 TeV [20], p+Pb at 5.02 TeV [21], and Pb+Pb at 2.76 TeV [22]. Dashed lines and the corresponding symbols correspond to model calculations; dash-dotted lines and their symbols apply similarly to the experimental results. The three vertical dashed lines correspond to the three multiplicities displayed in Fig. 1.

lision systems under consideration, for both the model hydrodynamic calculations and the corresponding experimental measurements, as functions of $(dN_{ch}/d\eta)^{1/3}$. For reference, vertical gray lines (dashed) have been added to indicate the three $dN_{ch}/d\eta$ values shown in Fig. 1. To guide the eye, fit lines have been added to each experimental (dashed) and hydrodynamic (dash-dotted) dataset. In the latter case, the fits are performed only in the five highest multiplicity bins where the effects of the wing-like freeze-out structure in small systems become apparent.

One finds in these results strong confirmation of the intuition provided by the above analysis of the pocket relations (4)-(6). There is an obvious non-universality in the slopes of R_o in large and small systems: for $K_T = 450$ MeV, the slope magnitudes in Fig. 3(a) are strongly ordered by collision size, and the hydrodynamic trends are in quite good qualitative agreement with those in the data. By contrast, virtually no splitting is visible in the R_s slopes [Fig. 3(b)], and the experimental slopes are again well reproduced by the model. Some larger model-to-data discrepancies are seen in the slopes of R_l [Fig. 3(c)] which are likely due to several simplifying assumptions in the model used here [26].² Most importantly, the qualitative agreement between the model and the data is remarkably good, given the simplicity of the model.

4. Discussion. Hydrodynamics naturally predicts en-

hanced collective flow in small systems due to larger initial density gradients over those present in large systems. This leads to measurable effects in the $(dN_{ch}/d\eta)^{1/3}$ -scaling of the HBT radii obtained from pion interferometry. Most notably, one observes the development of both a slope hierarchy between different radii in the same system and a slope non-universality when comparing the same radius across different collision systems. Both features are evident in the experimental data, which are qualitatively similar to the model results presented here.

The effects are strongest in R_o , which exhibits a strong splitting across different systems at intermediate K_T , while effects on R_l are qualitatively similar but less pronounced. Essentially no splitting is seen in the slopes of R_s , which is relatively insensitive to the temporal structure of the source distribution S [36].

Hydrodynamics thus provides a powerful and natural explanation of the disparate slopes in the various radii over a range of collision systems, by connecting it with the radical differences in transverse flow as a function of system size. The simple model used here (which is described more fully in Ref. [26]) provides quantitatively lacking, but qualitatively reasonable, agreement with experimental data. Because R_s and R_l as measured in the LCMS frame are dominated by geometric aspects of the source function S , they scale in a roughly monotonic fashion with $(dN_{ch}/d\eta)^{1/3}$. On the other hand, because R_o generally contains a mixture of both spatial and temporal information regarding S , the effects of violent collective expansion in small systems lead to strong distortions of the hydrodynamic freeze-out structure and much weaker resultant scaling with $(dN_{ch}/d\eta)^{1/3}$.

The $(dN_{ch}/d\eta)^{1/3}$ -dependence of the HBT radii thus

² The model generally overestimates the magnitudes of R_o and R_s but underestimates R_l , which is a consequence of the fact that preequilibrium flow has not been included here [26, 37].

presents a highly sensitive test for models of collectivity in nuclear collisions. When combined with suitably complementary momentum-space observables, it may even offer the ability to discriminate between existing models of collectivity. Future studies will explore these findings in the context of more realistic hydrodynamic models.

Acknowledgments. The author gratefully acknowledges the use of computing resources from Computing resources from both the Minnesota Supercomputing Institute (MSI) at the University of Minnesota and the Ohio Supercomputer Center [38]. C. P. acknowledges support from the CLASH project (KAW 2017-0036) and from the US-DOE Nuclear Science Grant No. DE-SC0019175.

* christopher.plumberg@gmail.com;

ORCID:

<https://orcid.org/0000-0001-6678-3966>

- [1] James L. Nagle and William A. Zajc. Small System Collectivity in Relativistic Hadronic and Nuclear Collisions. *Ann. Rev. Nucl. Part. Sci.*, 68:211–235, 2018, 1801.03477.
- [2] J. Adolfsson et al. QCD Challenges from pp to A-A Collisions. 3 2020, 2003.10997.
- [3] Mauricio Martinez, Matthew D. Sievert, and Douglas E. Wertepny. Multiparticle Production at Mid-Rapidity in the Color-Glass Condensate. *JHEP*, 02:024, 2019, 1808.04896.
- [4] Douglas Wertepny, Jacquelyn Noronha-Hostler, Matthew Sievert, Skandaprasad Rao, and Noah Paladino. Correlations in the Initial Conditions of Heavy-Ion Collisions. *EPJ Web Conf.*, 235:08002, 2020.
- [5] Zi-Wei Lin, Liang He, Terrence Edmonds, Feng Liu, Denes Molnar, and Fuqiang Wang. Elliptic Anisotropy v_2 May Be Dominated by Particle Escape instead of Hydrodynamic Flow. *Nucl. Phys. A*, 956:316–319, 2016, 1512.06465.
- [6] Christian Bierlich, Gösta Gustafson, and Leif Lönnblad. Collectivity without plasma in hadronic collisions. *Phys. Lett. B*, 779:58–63, 2018, 1710.09725.
- [7] Torbjörn Sjöstrand. Collective Effects: the viewpoint of HEP MC codes. *Nucl. Phys. A*, 982:43–49, 2019, 1808.03117.
- [8] Aleksi Kurkela, Urs Achim Wiedemann, and Bin Wu. Nearly isentropic flow at sizeable η/s . *Phys. Lett. B*, 783:274–279, 2018, 1803.02072.
- [9] Bjoern Schenke, Sangyong Jeon, and Charles Gale. (3+1)D hydrodynamic simulation of relativistic heavy-ion collisions. *Phys. Rev. C*, 82:014903, 2010, 1004.1408. Charles Gale, Sangyong Jeon, Björn Schenke, Prithwish Tribedy, and Raju Venugopalan. Event-by-event anisotropic flow in heavy-ion collisions from combined Yang-Mills and viscous fluid dynamics. *Phys. Rev. Lett.*, 110(1):012302, 2013, 1209.6330. Charles Gale, Sangyong Jeon, and Bjoern Schenke. Hydrodynamic Modeling of Heavy-Ion Collisions. *Int. J. Mod. Phys. A*, 28:1340011, 2013, 1301.5893.
- [10] Chun Shen, Zhi Qiu, Huichao Song, Jonah Bernhard, Steffen Bass, and Ulrich Heinz. The iEBE-VISHNU code package for relativistic heavy-ion collisions. *Comput. Phys. Commun.*, 199:61–85, 2016, 1409.8164.
- [11] Ryan D. Weller and Paul Romatschke. One fluid to rule them all: viscous hydrodynamic description of event-by-event central p+p, p+Pb and Pb+Pb collisions at $\sqrt{s} = 5.02$ TeV. *Phys. Lett. B*, 774:351–356, 2017, 1701.07145.
- [12] Bjoern Schenke, Chun Shen, and Prithwish Tribedy. Hybrid Color Glass Condensate and hydrodynamic description of the Relativistic Heavy Ion Collider small system scan. *Phys. Lett. B*, 803:135322, 2020, 1908.06212.
- [13] Jean-Yves Ollitrault. Anisotropy as a signature of transverse collective flow. *Phys. Rev. D*, 46:229–245, 1992. Jean-Yves Ollitrault. Collective flow from azimuthal correlations. *Nucl. Phys. A*, 590:561C–564C, 1995.
- [14] Sergei A. Voloshin. Transverse radial expansion in nuclear collisions and two particle correlations. *Phys. Lett. B*, 632:490–494, 2006, nucl-th/0312065.
- [15] Urs Achim Wiedemann and Ulrich W. Heinz. Particle interferometry for relativistic heavy ion collisions. *Phys. Rept.*, 319:145–230, 1999, nucl-th/9901094.
- [16] Michael Annan Lisa, Scott Pratt, Ron Soltz, and Urs Wiedemann. Femtoscopy in relativistic heavy ion collisions. *Ann. Rev. Nucl. Part. Sci.*, 55:357–402, 2005, nucl-ex/0505014.
- [17] S.V. Akkelin and Yu.M. Sinyukov. The HBT interferometry of expanding sources. *Phys. Lett. B*, 356:525–530, 1995.
- [18] Ulrich W. Heinz and Barbara V. Jacak. Two particle correlations in relativistic heavy ion collisions. *Ann. Rev. Nucl. Part. Sci.*, 49:529–579, 1999, nucl-th/9902020.
- [19] Adam Kisiel, Wojciech Broniowski, Mikolaj Chojnacki, and Wojciech Florkowski. Azimuthally-sensitive femtoscopy from RHIC to LHC in hydrodynamics with statistical hadronization. *Phys. Rev. C*, 79:014902, 2009, 0808.3363.
- [20] K. Aamodt et al. Femtoscopy of pp collisions at $\sqrt{s} = 0.9$ and 7 TeV at the LHC with two-pion Bose-Einstein correlations. *Phys. Rev. D*, 84:112004, 2011, 1101.3665.
- [21] J. Adam et al. Two-pion femtoscopy in p-Pb collisions at $\sqrt{s_{NN}} = 5.02$ TeV. *Phys. Rev. C*, 91:034906, 2015, 1502.00559.
- [22] Jaroslav Adam et al. Centrality dependence of pion freeze-out radii in Pb-Pb collisions at $\sqrt{s_{NN}} = 2.76$ TeV. *Phys. Rev. C*, 93(2):024905, 2016, 1507.06842.
- [23] M.I. Podgoretsky. On the Comparison of Identical Pion Correlations in Different Reference Frames. *Sov. J. Nucl. Phys.*, 37:272, 1983.
- [24] A. Kisiel. Femtoscopy of Pb-Pb and pp collisions at the LHC with the ALICE experiment. *J. Phys. G*, 38:124008, 2011, 1109.5553.
- [25] Łukasz Kamil Graczykowski. Pion femtoscopy measurements in ALICE at the LHC. *EPJ Web Conf.*, 71:00051, 2014, 1402.2138.
- [26] Christopher Plumberg. Hanbury Brown–Twiss Interferometry and Collectivity in p+p, p+Pb, and Pb+Pb Collisions (to be published in *Phys. Rev. C*). 8 2020, 2008.01709.
- [27] Ulrich W. Heinz and J. Scott Moreland. Hydrodynamic flow in small systems or: “How the heck is it possible that a system emitting only a dozen particles can be described by fluid dynamics?”. *J. Phys. Conf. Ser.*, 1271(1):012018, 2019, 1904.06592.
- [28] Urs Achim Wiedemann and Ulrich W. Heinz. Resonance contributions to HBT correlation radii. *Phys. Rev. C*, 56:3265–3286, 1997, nucl-th/9611031.
- [29] Yu.M. Sinyukov and Y.Yu. Tolstykh. Coherence influence

- on the Bose-Einstein correlations. *Z. Phys. C*, 61:593–597, 1994.
- Yu.M. Sinyukov and V.M. Shapoval. Correlation femtoscopy of small systems. *Phys. Rev. D*, 87(9):094024, 2013, 1209.1747.
- S.V. Akkelin and Yu.M. Sinyukov. Simple estimates of non-femtoscopic particle correlations in $p + p$ collisions. *Phys. Part. Nucl. Lett.*, 8(9):959–964, 2011.
- V.M. Shapoval, P. Braun-Munzinger, Iu. A. Karpenko, and Yu. M. Sinyukov. Femtoscopic scales in $p + p$ and $p + \text{Pb}$ collisions in view of the uncertainty principle. *Phys. Lett. B*, 725:139–147, 2013, 1304.3815.
- [30] Ulrich W. Heinz. Hanbury-Brown/Twiss interferometry for relativistic heavy ion collisions: Theoretical aspects. In *International Summer School on Correlations and Clustering Phenomena in Subatomic Physics*, pages 137–177, 8 1996, nucl-th/9609029.
- [31] Christopher Plumberg and Ulrich Heinz. Hanbury-Brown–Twiss correlation functions and radii from event-by-event hydrodynamics. *Phys. Rev. C*, 98(3):034910, 2018, 1611.03161.
- [32] Ulrich W. Heinz. Concepts of heavy ion physics. In *2nd CERN-CLAF School of High Energy Physics*, pages 165–238, 7 2004, hep-ph/0407360.
- [33] Christopher Plumberg and Ulrich Heinz. Interferometric signatures of the temperature dependence of the specific shear viscosity in heavy-ion collisions. *Phys. Rev. C*, 91(5):054905, 2015, 1503.05605.
- [34] C. Loizides, J. Nagle, and P. Steinberg. Improved version of the PHOBOS Glauber Monte Carlo. *SoftwareX*, 1-2:13–18, 2015, 1408.2549.
- Piotr Bożek, Wojciech Broniowski, Maciej Rybczynski, and Grzegorz Stefanek. GLISSANDO 3: GLauber Initial-State Simulation AND mOre..., ver. 3. *Comput. Phys. Commun.*, 245:106850, 2019, 1901.04484.
- [35] T. Csörgő and S. Pratt. Structure of the peak in Bose-Einstein correlations. *Conf. Proc. C*, 9106175:75–90, 1991.
- [36] Scott Chapman, Pierre Scotto, and Ulrich W. Heinz. Model independent features of the two particle correlation function. *Acta Phys. Hung. A*, 1:1–31, 1995, hep-ph/9409349.
- [37] Scott Pratt. Resolving the HBT Puzzle in Relativistic Heavy Ion Collision. *Phys. Rev. Lett.*, 102:232301, 2009, 0811.3363.
- [38] Ohio Supercomputer Center. Ohio supercomputer center, 1987.